Catalysis Today 176 (2011) 292–297

Contents lists available at ScienceDirect

Catalysis Today

journal homepage: www.elsevier.com/locate/cattod

Heteropoly acid promoted Cu and Fe catalysts for the selective catalytic reduction of NO with ammonia

Siva Sankar Reddy Putluru, Susanne Mossin, Anders Riisager, Rasmus Fehrmann*

Centre for Catalysis and Sustainable Chemistry, Department of Chemistry, Building 207, Technical University of Denmark, DK-2800 Kgs. Lyngby, Denmark

ARTICLE INFO

Article history:
Received 29 September 2010
Received in revised form
26 November 2010
Accepted 30 November 2010
Available online 14 January 2011

Keywords:
HPA
SCR with ammonia
Potassium poisoning
Deactivation
NH_3-TPD

ABSTRACT

Cu/TiO_2, Fe/TiO_2 and heteropoly acid promoted Cu/TiO_2, Fe/TiO_2 catalysts were prepared and characterized by N_2 physisorption, XRPD, NH_3-TPD, H_2-TPR and EPR. The catalysts exhibited only crystalline TiO_2 phases with the active metals and promoters in highly dispersed state. The acidic properties were studied and compared with the catalytic activity for the selective catalytic reduction (SCR) of NO with ammonia. The SCR activities and acidity values of heteropoly acid promoted catalysts were found to be much higher than unpromoted catalysts. The influence of potassium poisons on the SCR activity and acidity was lower for promoted catalysts than for unpromoted catalysts. In the heteropoly acid promoted catalysts the SCR active Cu and Fe metals were protected from potassium poisons by bonding of the potassium to the Brønsted acid centres. Thus heteropoly acid promoted catalysts might be suitable for biomass fired power plant SCR applications.

1. Introduction

Today, catalysis by heteropoly acids (HPAs) is well established and applications in both heterogeneous and homogeneous systems have been reviewed by many researchers [1–10]. Additionally, several industrial processes based on HPAs have been developed and commercialized [1,4–8] including acid catalysis and catalytic oxidation as two major areas. HPAs have unique physicochemical properties, with structural mobility and multi functionality as the most important for catalysis [1–3]. Importantly, they also possess, a very strong Brønsted acidity and redox properties, which can be tuned by varying the chemical composition [3]. Often the strong Brønsted acidity, greatly exceeding that of ordinary mineral acids and solid acid catalysts provide HPAs with higher activity, selectivity and cleaner processing compared to conventional catalysts [8].

There are many structural types of HPAs [9]. The majority of catalytic applications are based on the most stable and easily available Keggin HPAs, especially for acid catalysis. For practical applications, it is important to improve the physical properties of HPAs (e.g., mechanical and thermal resistance). This might be reached by depositing HPAs on a suitable support (e.g., TiO_2 or ZrO_2). Supported HPAs also provide increased surface area when compared to bulk HPAs.

Flue gases from stationary sources such as power plants contain CO, NO_x and hydrocarbons. The conversion of these pollutants to CO_2, N_2 and H_2O using catalysts is a challenge. HPAs have been reported to be active for flue gas cleaning [10–15]. Thus it has been found that the 12-tungstophosphoric acid (TPA) can effectively absorb NO at flue gas temperatures, and upon rapid heating, the absorbed NO is effectively decomposed into N_2 [10,11]. Pt/TPA and TPA supported metal oxides were also used extensively for the abatement of NO_x for mobile applications [12,13], e.g., Pd loaded on dispersed $H_3PW_{12}O_{40}$ (TPA) on a SiO_2 carrier was applied for selective reduction of NO with aromatic hydrocarbons [14,15].

Selective catalytic reduction (SCR) of NO_x in flue gases with NH_3 on V_2O_5–WO_3/TiO_2 is very successful in industrial plants [16–19]. The anatase form of TiO_2 is the support of choice due to higher surface area compared to the rutile phase. TiO_2 is also chosen because SO_3 from the oxidation of SO_2 in the flue gas does not deteriate the TiO_2 carrier. The V_2O_5–WO_3/TiO_2 catalyst does, however, have some limitations regarding toxicity, stability and selectivity at higher temperatures [20].

Conventional vanadia based catalysts are susceptible to poisoning by alkali metals [21–23]. This is a significant drawback in the combustion of alkali rich fuels like straw and other types of biomass. Biomass is considered a CO_2 neutral fuel giving back to the atmosphere what was accumulated during growth. Biomass is thus increasingly used as co-fuel in coal fired power plants. The problem of alkali poisoning has intensified the search for alternative SCR catalysts with a greater alkali tolerance. Potential alternatives to the V_2O_5 catalysts are Cu and Fe metal oxides

* Corresponding author. Tel.: +45 45252389; fax: +45 45883136.
E-mail address: rf@kemi.dtu.dk (R. Fehrmann).

0920-5861/$ – see front matter © 2011 Elsevier B.V. All rights reserved.
doi:10.1016/j.cattod.2010.11.087

which furthermore also are less toxic [20]. One of the possible ways to increase catalyst resistance to alkaline poisons is the use of supports, revealing high or super-acidic properties which would interact stronger with alkali than the active metal oxide species. Such super-acidic properties are characteristic of HPAs [24].

In the present work, we have studied the promotional effect and alkali resistance of heteropoly acids supported on TiO_2 with Cu and Fe oxide as SCR catalysts and with NH_3 as the reducing agent. The influence of potassium oxide loading on the activity was also studied and compared with unpromoted Cu/TiO_2 and Fe/TiO_2 SCR catalysts. All the catalysts were characterized by various techniques to allow detailed discussion of the SCR performance.

2. Experimental

2.1. Catalyst preparation and characterization

TiO_2 supported heteropoly acids $H_3PW_{12}O_{40}$ (TPA), $H_4SiW_{12}O_{40}$ (TSiA), and $H_3PMo_{12}O_{40}$ (MPA) (Aldrich, 99.99%) were prepared by suspending a known amount of dried TiO_2 anatase powder (Aldrich, 99.7%) in aqueous solution of corresponding heteropoly acids. The suspended mixtures (optimum heteropoly acid loading, 15 wt.%) were evaporated and then dried at 120 °C for 12 h [25]. 3 wt.% Cu and 3 wt.% Fe modified catalysts were prepared by wet impregnation by dissolving the required amount of copper nitrate (Aldrich, 99.99%) and iron nitrate (Aldrich, 99.9%) as a precursor in water with the pure TiO_2 and heteropoly acid–TiO_2 supports. The potassium-doped catalyst was prepared by co-impregnation with a solution of KNO_3 (Aldrich, 99.99%) to obtain a potassium loading of 100 μmol/g catalyst. Each impregnated catalyst was oven dried at 120 °C for 12 h followed by calcination at 400 °C for 4 h prior to use.

X-ray powder diffraction (XRPD) measurements were performed on a Huber G670 powder diffractometer using Cu Kα radiation within a 2θ range of 10–60° in steps of 0.02°. The BET surface area of the samples was determined from nitrogen physisorption measurements on about 100 mg sample at liquid nitrogen temperature with a Micromeritics ASAP 2010 instrument. The samples were heated to 200 °C for 1 h prior to the measurements.

NH_3-TPD experiments were conducted on a Micromeritics Autochem-II instrument. In a typical TPD experiment, 100 mg of dried sample was placed in a quartz tube and pretreated in flowing He at 500 °C for 2 h. Then, the temperature was lowered to 100 °C and the sample was treated with anhydrous NH_3 gas (Air Liquide, 5% NH_3 in He). After NH_3 adsorption, the sample was flushed with He (50 ml/min) for 100 min at 100 °C. Finally, the TPD measurement was carried out by heating the sample from 100 to 700 °C (10 °C/min) under a flow of He (25 ml/min).

H_2-TPR studies were also conducted on a Micromeritics Autochem-II instrument. In a typical experiment, 100 mg of an oven-dried sample was placed in one arm of a U-shaped quartz tube on a quartz wool plug. Prior to TPR, the catalyst sample was pretreated by flushing with air at 300 °C for 2 h. After pretreatment, the sample was cooled to ambient temperature and the TPR analysis carried out in a reducing mixture (50 ml/min) consisting of 5% H_2 and balance Ar (Air Liquide) from ambient temperature to 1000 °C (10 °C/min). The hydrogen concentration in the effluent stream was monitored by a thermal conductivity detector (TCD).

EPR spectra of the catalysts were recorded ex situ with a Bruker EMX-EPR spectrometer, working in the X-band (Bruker ER 041 XGG Microwave Bridge) at microwave frequencies around 9.75 GHz. The measurements were done at room temperature on samples transferred directly after calcination into a desiccator. Data treatment was performed with WIN-EPR software provided by Bruker.

2.2. Catalytic activity measurements

The SCR activity measurements were carried out at atmospheric pressure in a fixed-bed quartz reactor loaded with 20 mg of fractionized (180–300 μm) catalyst samples positioned between two layers of inert quartz wool. The reactant gas composition was adjusted to 1000 ppm NO, 1100 ppm NH_3, 3.5% O_2, 2.3% H_2O and balance N_2 by mixing 1% NO/N_2 (±0.1% abs.), 1% NH_3/N_2 (±0.005% abs.), O_2 (≥99.95%) and balance N_2 (≥99.999%) (Air Liquide) using Bronkhorst EL-Flow F-201C/D mass-flow controllers. The total flow rate was maintained at 500 ml/min (ambient conditions). During the experiments the temperature was increased stepwise from 200 °C while the NO and NH_3 concentrations were continuously monitored by a Thermo Electron Model 17C chemiluminiscent NH_3-NO_x gas analyzer. All measurements were recorded after steady state was obtained (approximately obtained after 45–60 min).

The catalytic activity is represented as the first-order rate constant ($cm^3/g\,s$), since the SCR reaction is known to be first-order with respect to NO under stoichiometric NH_3 conditions [26]. The first-order rate constants under plug flow conditions were thus obtained from Eq. (1):

$$k = -\left(\frac{F_{NO}}{m_{cat} \cdot C_{NO}}\right) \ln(1 - X) \quad (1)$$

where F_{NO} denotes the molar feed rate of NO (mol/s), m_{cat} the catalyst weight (g), C_{NO} the NO concentration (mol/cm^3) in the inlet gas and X the fractional conversion of NO.

The catalyst amount was kept sufficient low to secure that the measured conversions were well below 90% at all temperatures.

3. Results and discussion

The XRPD patterns of Cu–Ti and Fe–Ti based catalysts with and without HPA promoters are shown in Fig. 1. Only diffractions corresponding to the TiO_2 support can be observed indicating that CuO or Fe_2O_3 are highly dispersed in an amorphous state on the surface of the support. Furthermore, absence of phases of HPAs or their decomposition products (like MoO_3 and WO_3) suggests that also HPAs are highly dispersed and thermally stable at the calcination temperature of 400 °C. This is in accordance with literature data where thermal stability up to 700 °C has been reported [27]. Potassium-doped catalysts show similar XRPD patterns as the corresponding undoped catalysts (not shown in figure). BET surface areas of the Cu and Fe based catalysts are presented in Table 1. The surface areas of the Cu–Ti and Fe–Ti catalysts were measured to be 128 and 120 m^2/g, respectively, while the areas of the HPA-promoted catalysts were slightly lower in the range of 90–110 m^2/g.

NH_3-TPD is used to evaluate the acidity of the catalysts. The ammonia desorption profiles of both the Cu- and Fe-impregnated catalysts and corresponding potassium-doped samples are pre-

Table 1
Surface area and NH_3-TPD results of Cu and Fe based catalysts.

Catalyst	Surface area (m^2/g)	Acidity (μmol/g)		T_{max} of desorption (°C)	
		Fresh	K-doped	Fresh	K-doped
Cu–Ti	128	490	190	291	288
Cu–MPA–Ti	95	687	455	349	316
Cu–TPA–Ti	108	745	536	386	341
Cu–TSiA–Ti	115	630	514	405	338
Fe–Ti	122	452	200	293	291
Fe–MPA–Ti	92	709	515	380	342
Fe–TPA–Ti	100	613	505	412	347
Fe–TSiA–Ti	108	683	540	419	344

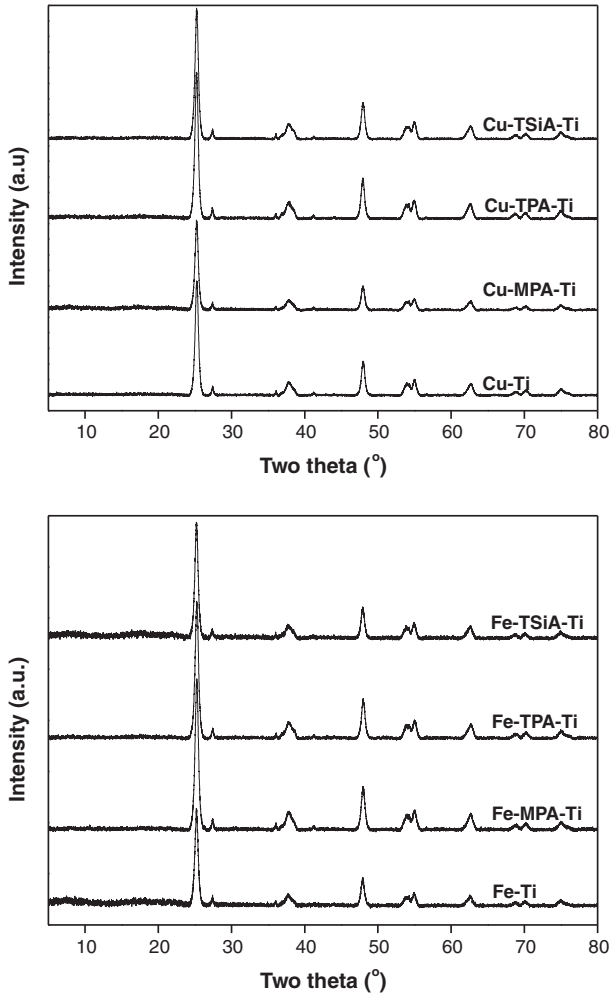

Fig. 1. XRPD patterns of Cu and Fe based catalysts.

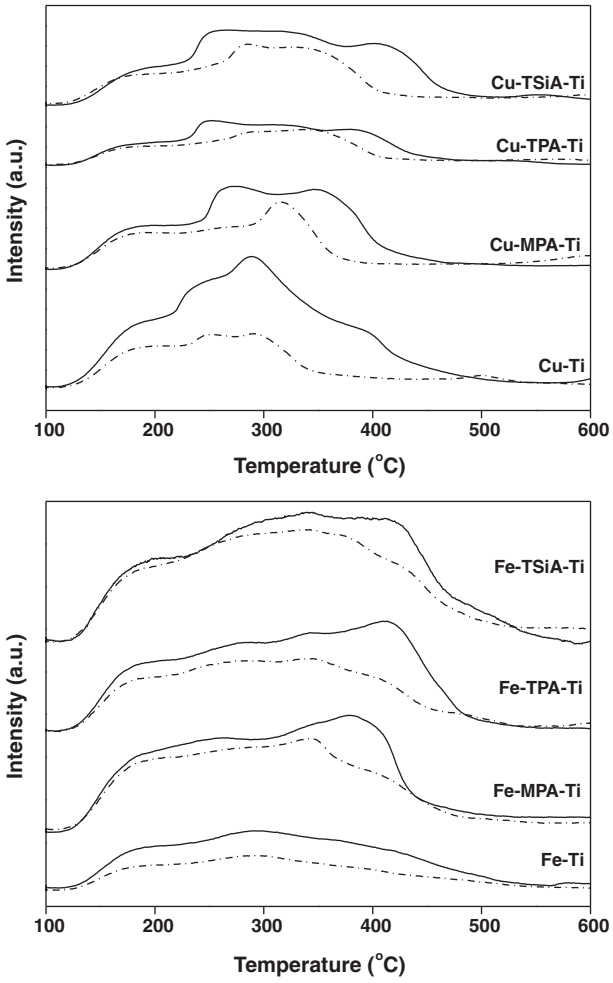

Fig. 2. NH_3-TPD profiles of fresh (thick line) and potassium doped (dotted line) Cu and Fe based catalysts.

sented in Fig. 2. For all samples the total amount of desorbed ammonia and T_{max} of desorption are listed in Table 1. The total amount of adsorbed ammonia corresponds to molecular adsorbed ammonia or ammonium ions on Lewis or Brønsted acid sites [28]. The relative strength of the acid sites are reflected by the temperature of maximum ammonia desorption. The NH_3-TPD profile of the fresh Cu–Ti and Fe–Ti catalysts showed primarily a sharp desorption temperature peak around 290 °C, whereas the Cu–HPA–Ti and Fe–HPA–Ti catalysts showed a broad desorption T_{max} peak above 350 °C, which probably is due to Brønsted acid sites from the HPAs. As calculated in Table 1, Cu–Ti and Fe–Ti catalysts have total acidities of 490 and 452 μmol/g, respectively, whereas Cu–HPA–Ti and Fe–HPA–Ti catalysts are more acidic with values above 613 μmol/g due to the super acidic nature of the HPA promoters. The acid strength of the fresh HPA-promoted samples with Cu follows the order: Cu–TSiA–Ti > Cu–TPA–Ti > Cu–MPA–Ti > Cu–Ti, whereas the surface acidity is ranked in the order: Cu–TPA–Ti > Cu–MPA–Ti > Cu–TSiA–Ti > Cu–Ti. Fresh Fe–HPA–Ti catalysts showed similar acid strength as that of Cu–HPA–Ti catalysts, whereas the surface acidity of the iron based catalysts is in the order: Fe–MPA–Ti > Fe–TSiA–Ti > Fe–TPA–Ti > Fe–Ti. Thus, HPA-promoted catalysts show high surface acidity and acid strength compared to unpromoted catalysts.

The NH_3 desorption profiles of the potassium-poisoned catalysts showed an overall decrease in surface acidity as reported in Table 1. Moreover, the alkali doping is associated with a decrease in acid strength on all catalysts, in agreement with earlier reports [21,22,28]. The weakening of the acid sites is due to occupation of potassium on the strongest acid sites, which decreases the strength of the remaining acid sites through electron donation. Especially KCu–Ti and KFe–Ti catalysts showed an acidity drop of 61% and 55%, respectively. In comparison the acidity of the HPA-promoted catalysts decreased 33% upon potassium-doping. Similar alkali resistivity results were observed on TiO_2 and ZrO_2 surface modified catalysts [28,29].

H_2-TPR is frequently used to study the redox property of metal oxide catalysts. In Fig. 3 the TPR patterns of both fresh and potassium-doped Cu and Fe catalysts are shown. All the Cu catalysts showed three reduction peaks: a sharp low temperature peak with maximum between 100 and 200 °C, a small shoulder at medium temperature around 300 °C and a broad high temperature peak between 560 and 730 °C. Cu–Ti catalysts yielded only low and medium temperature peaks while all three peaks were observed in Cu–HPA–Ti catalysts. The high temperature peak is due to the reduction of polymeric MoO_3 or WO_3 [30,31], whereas the low and medium temperature peaks are ascribed to reduction of CuO [32,33]. In more detail, the two or three reduction peaks observed for the Cu catalysts in the low temperature region, can be ascribed to sequential reduction of CuO species on the TiO_2 support, while the medium temperature reduction peak has been attributed to interacting or anchored CuO on TiO_2 [32,33].

Potassium-doped Cu catalysts showed similar H_2-TPR profiles with some changes in reduction temperatures as indicated in Table 2. Hence, in the Cu–Ti catalyst the T_{max} position of the low

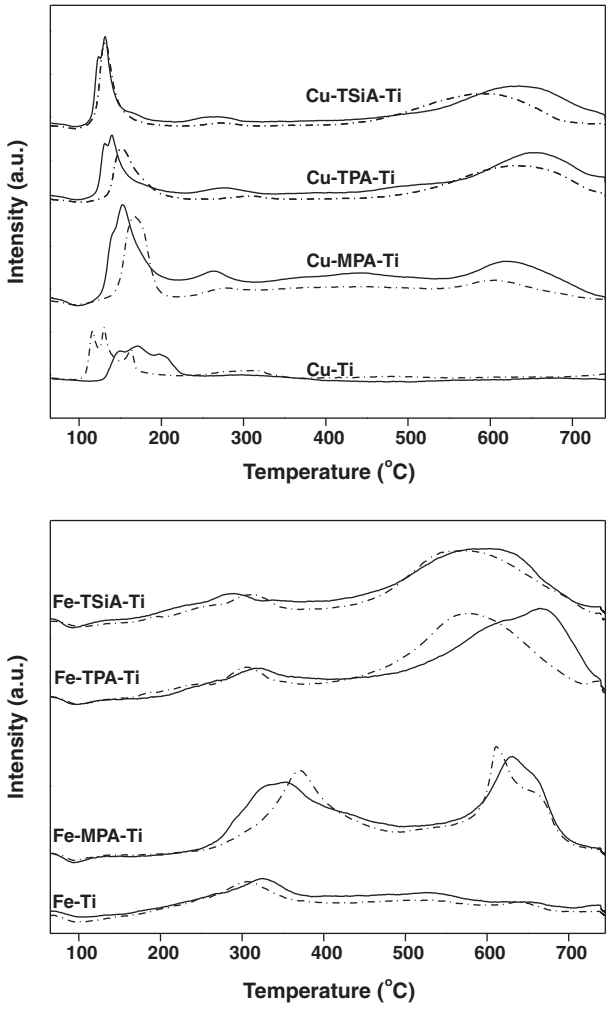

Fig. 3. H_2-TPR profiles of fresh (thick line) and potassium doped (dotted line) Cu and Fe based catalysts.

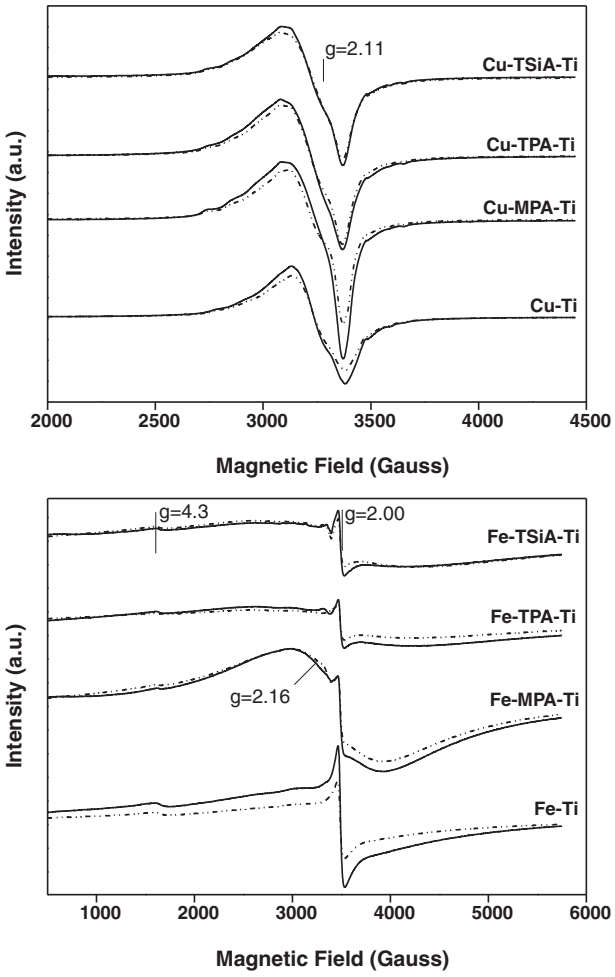

Fig. 4. X-band EPR spectra of fresh (thick line) and potassium doped (dotted line) Cu and Fe based catalysts recorded at room temperature.

temperature reduction is decreased from 171 to 130 °C, whereas increased or unchanged T_{max} reduction temperatures were found for Cu–HPA–Ti catalysts upon potassium addition. In contrast, the high temperature reduction peaks in Cu–HPA–Ti catalysts are decreased upon potassium addition, indicating that the active Cu species are protected from the potassium species in the promoted catalysts. The Fe–Ti catalyst revealed only one reduction peak and Fe–HPA–Ti catalysts two reduction peaks. The low temperature peak around 300–320 °C is ascribed to iron oxide reduction [34]. Potassium doped Fe catalysts also showed similar shift in low and high temperature T_{max} position as observed with the Cu catalysts.

The H_2 consumption values of both fresh and potassium-doped Cu and Fe catalysts are shown Table 2. Cu–Ti and Fe–Ti catalysts have a H_2 consumption of 752 and 843 μmol/g, respectively, whereas Cu–HPA–Ti and Fe–HPA–Ti catalysts are showing high H_2 consumption with values above 2000 μmol/g due to the reduction of polymeric MoO_3 and WO_3. Potassium-doped Cu and Fe catalysts showed a decrease in H_2 consumption (25–30 μmol/g) compared to the fresh catalysts.

Fig. 4 shows EPR spectra of the fresh and potassium-doped Cu and Fe based catalysts. In the spectra of the Cu catalysts a spectral parameter value at $g = 2.11$ can be interpreted as resulting from

Table 2
H_2-TPR results of Cu and Fe based catalysts.

Catalyst	Low temperature peak (°C)		High temperature peak (°C)		H_2 consumption (μmol/g)	
	Fresh	K-doped	Fresh	K-doped	Fresh	K-doped
Cu–Ti	171	130	–	–	752	722
Cu–MPA–Ti	154	166	621	602	2695	2668
Cu–TPA–Ti	141	151	656	633	2095	2073
Cu–TSiA–Ti	132	132	637	587	2011	1982
Fe–Ti	325	306	–	–	843	818
Fe–MPA–Ti	352	369	632	610	2704	2677
Fe–TPA–Ti	313	309	666	578	2109	2079
Fe–TSiA–Ti	286	310	595	569	2161	2140

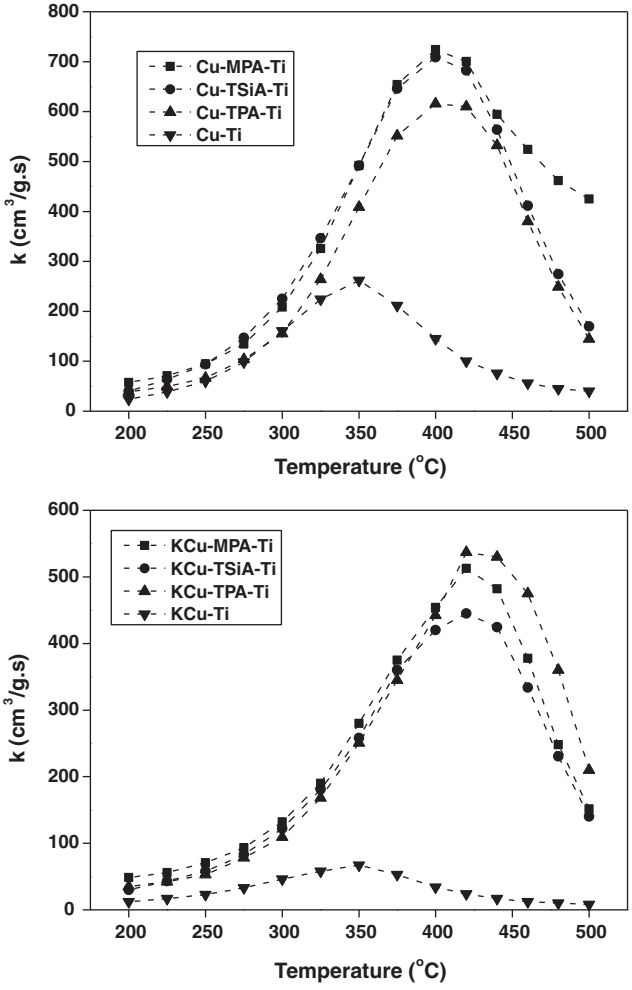

Fig. 5. Temperature dependency of first-order rate constant for SCR of NO with fresh and potassium doped Cu based catalysts. Reaction conditions: 1000 ppm NO, 1100 ppm NH_3, 3.5% O_2, 2.3% H_2O, and balance N_2.

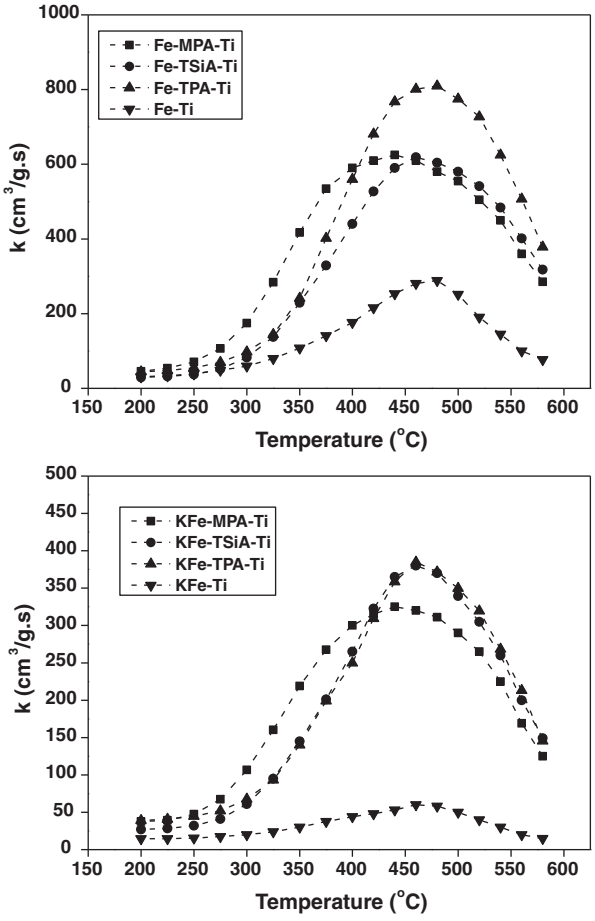

Fig. 6. Temperature dependency of first-order rate constant for SCR of NO with fresh and potassium doped Fe based catalysts. Reaction conditions: 1000 ppm NO, 1100 ppm NH_3, 3.5% O_2, 2.3% H_2O, and balance N_2.

distorted octahedrally coordinated Cu^{2+} ions [35], and the hyperfine splitting indicates the existence of isolated Cu^{2+} ions on the support [36]. Fe-based catalysts showed intense spectral values at $g = 2.00$ and $g = 4.30$ ascribed to isolated octahedral and rhombic Fe^{3+} in anatase, respectively [34]. In the spectra of the Fe–MPA–Ti catalyst an additional spectral value at $g = 2.16$ can be assigned to Fe^{3+} in Fe_2O_3-type clusters [34]. Potassium-doped Cu and Fe catalysts (dotted lines) showed similar spectral parameters with little decrease in intensity, thus making it difficult by EPR to determine the structural effect imposed by introduction of the alkali metal.

Overall XRPD and EPR characterization results reveal that all the catalysts showed similar spectral parameters with minor decrease in intensity after doping with potassium. Unpromoted Cu–Ti and Fe–Ti catalysts showed altered H_2-reduction and NH_3 desorption patterns, whereas promoted HPA catalysts showed similar reduction patterns and slightly altered desorption patterns after poisoning. Irrespective of the promotional effect small decrease of H_2 consumption (25–30 μmol/g) was observed after doping with potassium. Unpromoted catalysts showed substantial loss of initial acidity, whereas promoted HPA catalysts showed small loss of acidity.

The SCR activity of the fresh and potassium-doped Cu catalysts was measured in the temperature range 200–500 °C. In Fig. 5 the measured catalytic activities are reported as first-order mass based rate constants k ($cm^3/g\,s$). The catalytic activity is generally increasing with catalyst temperature until an optimum temperature is reached between 350 and 400 °C. Upon further increase in temperature the SCR activity decreases due to predominant ammonia oxidation [37,38]. HPA-promoted catalysts showed higher activity compared to that of unpromoted Cu–Ti catalyst with an relative order corresponding to Cu–MPA–Ti ≈ Cu–TSiA–Ti > Cu–TPA–Ti > Cu–Ti. Thus, Cu–MPA–Ti, Cu–TSiA–Ti, Cu–TPA–Ti and Cu–Ti catalysts showed k_{max} values of 724, 709, 616 and 262 $cm^3/g\,s$, respectively, at their T_{max} temperatures. These rate constants correspond to conversion values of 82.6% (Cu–MPA–Ti), 81.8% (Cu–TSiA–Ti), 77.2% (Cu–TPA–Ti) and 46.7% (Cu–Ti), respectively, using 20 mg of catalyst. No reports are available in the literature for the SCR of NO with NH_3 on HPA promoted catalysts for direct comparison with the observed values. However, Yoshimoto et al. [15] found low NO conversion and N_2 selectivity in SCR performed with various aromatic hydrocarbons on Pd–TPA/SiO_2. Potassium-doped Cu based catalysts (100 μmol K/g) was less active than the undoped catalysts showing k_{max} values of 513, 445, 537 and 67 $cm^3/g\,s$ for KCu–MPA–Ti, KCu–TSiA–Ti, KCu–TPA–Ti and KCu–Ti catalysts, respectively, at their T_{max} temperatures. Importantly, some of the rate constants are higher than obtained with the commercial V_2O_5–WO_3/TiO_2 catalyst and the highly alkali resistant V_2O_5/sulphated-ZrO_2 catalysts (430 $cm^3/g\,s$) under identical reaction conditions [22,28].

The SCR activity of the fresh and potassium-doped Fe catalysts were measured in the temperature range 200–580 °C (Fig. 6). Fe-based catalysts are showing maximum catalytic activity at higher temperatures (440–480 °C) compared to that of Cu based cata-

lysts. The order of catalytic activity (k_{max}) of fresh catalysts is: Fe–TPA–Ti (810 $cm^3/g\,s$) > Fe–MPA–Ti (625 $cm^3/g\,s$) > Fe–TSiA–Ti (619 $cm^3/g\,s$) > Fe–Ti (288 $cm^3/g\,s$) at T_{max} temperatures. These rate constants correspond to conversion values of 85.8% (Fe–TPA–Ti), 77.7% (Fe–MPA–Ti), 77.4% (Fe–TSiA–Ti) and 50.0% (Fe–Ti), respectively, using 20 mg of catalyst. This order is different from the one observed for the Cu catalysts where the molybdenum-containing MPA was the most active catalyst. Potassium-doping of the Fe catalysts also resulted in decrease of SCR activity resulting in k_{max} values at T_{max} temperature of 325, 380, 385 and 60 $cm^3/g\,s$ for KFe–MPA–Ti, KFe–TSiA–Ti, KFe–TPA–Ti and KFe–Ti catalysts, respectively. The observed change in catalytic activity after doping with potassium seems to correlate well with the total acidity of the catalysts (listed in Table 1). The loss of more than one mole of acid sites, estimated from the uptake of NH_3, per mole of potassium added might be due to partly coordination of K_2O to Cu and Fe along with interaction with HPAs and TiO_2 reducing the number of acid sites. This is also in accordance with Fig. 2 where the NH_3-TPD peaks are changed from broad shape to slightly narrow shape after doping with potassium.

The decrease in activity after potassium doping is represented as relative activity (%). Cu–Ti catalysts possessed a relative activity of 23% at 400 °C, whereas Cu–MPA–Ti, Cu–TSiA–Ti and Cu–TPA–Ti catalysts showed 63, 59 and 72%, respectively. Similarly, the Fe–Ti, Fe–MPA–Ti, Fe–TSiA–Ti and Fe–TPA–Ti catalysts showed a relative activity of 25, 51, 60 and 45%, respectively at 400 °C. Notably, these potassium deactivation values are significantly lower compared to those of traditional SCR catalysts. Highly active V_2O_5–WO_x/ZrO_2 catalysts reported in the literature for biomass fired applications also showed severe deactivation [22,28]. Hence, overall the HPA promoted catalysts are all very active and resistant to alkali poisoning compared to unpromoted catalysts.

4. Conclusions

Distribution of the heteropoly acids, MPA, TPA or TSiA on Cu–Ti and Fe–Ti entailed a substantial increase in acid strength and surface acidity. All the HPA promoted catalysts exhibited better SCR activity than unpromoted catalysts. Furthermore, the impact of potassium doping (100 μmol/g) on the Cu–HPA–Ti and Fe–HPA–Ti catalysts is less severe than found on the corresponding unpromoted Cu–Ti and Fe–Ti catalysts. Accordingly, heteropoly acid promoted Cu/TiO_2 and Fe/TiO_2 catalysts are promising new, SCR catalysts for flue gas cleaning in both coal and biomass fired power plant installations.

Acknowledgements

Energinet.dk is thanked for financial support of this work through the PSO project FU7318. Dong Energy A/S and Vattenfall A/S for their financial contribution as well.

References

[1] T. Okuhara, N. Mizuno, M. Misono, Adv. Catal. 41 (1996) 113.
[2] I.V. Kozhevnikov, Chem. Rev. 98 (1998) 171.
[3] J.B. Moffat, Metal–Oxygen Clusters: The Surface and Catalytic Properties of Heteropoly Oxometalates, Kluwer, New York, 2001.
[4] Y. Izumi, K. Urabe, M. Onaka, Zeolite, Clay, and Heteropoly Acid in Organic Reactions, VCH, Weinheim, 1992.
[5] A. Corma, Chem. Rev. 95 (1995) 559.
[6] T. Okuhara, N. Mizuno, M. Misono, Appl. Catal. A 222 (2001) 63.
[7] I.V. Kozhevnikov, Catalysts for Fine Chemicals, vol. 2: Catalysis by Polyoxometalates, Wiley, Chichester, England, 2002.
[8] M.N. Timofeeva, Appl. Catal. A 256 (2003) 19.
[9] M.T. Pope, Heteropoly and Isopoly Oxometalates, Springer, Berlin, 1983.
[10] R.T. Yang, N. Chen, Ind. Eng. Chem. Res. 33 (1994) 825.
[11] R. Belanger, J.B. Moffat, J. Catal. 152 (1995) 179.
[12] K. Vaezzadeh, C. Petit, V. Pitchon, Catal. Today 73 (2002) 297.
[13] M.A. Gomez-Garcia, V. Pitchon, A. Kiennemann, Catal. Today 107 (2005) 60.
[14] K. Okumura, R. Yoshimoto, K. Suzuki, M. Niwa, Bull. Chem. Soc. Jpn. 78 (2005) 361.
[15] R. Yoshimoto, T. Ninomiya, K. Okumura, M. Niwa, Appl. Catal. B 75 (2007) 175.
[16] S.C. Wood, Chem. Eng. Prog. 90 (1994) 32.
[17] H. Bosch, F.J.J.G. Janssen, Catal. Today 2 (1998) 5.
[18] S.M. Cho, Chem. Eng. Prog. 90 (1994) 39.
[19] P. Forzatti, L. Lietti, Heterogen. Chem. Rev. 3 (1996) 33.
[20] S. Brandenberger, O. Kröcher, A. Tissler, R. Althoff, Catal. Rev. 50 (2008) 492.
[21] J.P. Chen, R.T. Yang, J. Catal. 125 (1990) 411.
[22] J. Due-Hansen, S. Boghosian, A. Kustov, P. Fristrup, G. Tsilomelekis, K. Ståhl, C.H. Christensen, R. Fehrmann, J. Catal. 251 (2007) 459.
[23] Y. Zheng, A.D. Jensen, I.E. Johnsson, Ind. Eng. Chem. Res. 43 (2004) 941.
[24] R.S. Drago, J.A. Dias, T. Maier, J. Am. Chem. Soc. 119 (1997) 7702.
[25] B.M. Devassy, S.B. Halligudi, J. Catal. 236 (2005) 313.
[26] R.Q. Long, R.T. Yang, J. Catal. 196 (2000) 73.
[27] S.M. Kumbar, G.V. Shanbhag, F. Lefebvre, S.B. Halligudi, J. Mol. Catal. A 256 (2006) 324.
[28] A.L. Kustov, M.Yu. Kustova, R. Fehrmann, P. Simonsen, Appl. Catal. B 58 (2005) 97.
[29] A.L. Kustov, S.B. Rasmussen, R. Fehrmann, P. Simonsen, Appl. Catal. B 76 (2007) 9.
[30] A.A. Spojakina, N.G. Kostova, B. Sow, M.W. Stamenova, K. Jiratova, Catal. Today 65 (2011) 315.
[31] L.M. Gomez Sainero, S. Damyanova, J.L.G. Fierro, Appl. Catal. A 208 (2001) 63.
[32] S. Guerrero, I. Guzmán, G. Aguila, P. Araya, Catal. Commun. 11 (2009) 38.
[33] J. Xiaoyuan, D. Guanghui, L. Liping, C. Yingxu, Z. Xiaoming, J. Mol. Catal. A 218 (2004) 187.
[34] G. Pecchi, P. Reyes, J. Sol–Gel Sci. Technol. 27 (2003) 205.
[35] W. Dow, P. Wang, T. Huang, J. Catal. 160 (1996) 155.
[36] P. Ratnasamy, D. Srinivas, C.V.V. Satyanarayana, P. Manikandan, R.S. Senthil Kumaran, M. Sachin, J. Catal. 221 (2004) 455.
[37] G. Ramis, L. Yi, G. Busca, M. Turco, E. Kotur, R.J. Willey, J. Catal. 157 (1995) 523.
[38] R.Q. Long, R.T. Yang, J. Catal. 186 (1999) 254.